OPEN ACCESS

Repository of the Max Delbrück Center for Molecular Medicine (MDC) in the Helmholtz Association

http://edoc.mdc-berlin.de/14670

Quantification of the transmural dynamics of atrial fibrillation by simultaneous endocardial and epicardial optical mapping in an acute sheep model

Gutbrod, S.R., Walton, R., Gilbert, S., Meillet, V., Jais, P., Hocini, M., Haissaguerre, M., Dubois, R., Bernus, O., Efimov, I.

This is the final version of the accepted manuscript. The original article has been published in final edited form in:

Circulation Arrhythmia and Electrophysiology
2015 APR; 8(2): 456-465
2015 FEB 24 (originally published online)
doi: 10.1161/CIRCEP.114.002545
Publisher: American Heart Association

© 2015 American Heart Association, Inc.

Quantification of the Transmural Dynamics of Atrial Fibrillation by Simultaneous Endocardial and Epicardial Optical Mapping in an Acute Sheep Model

Running title: *Gutbrod et al.; Atrial Fibrillation Transmural Dynamics*

Sarah R. Gutbrod, MS[1,2]; Richard Walton, PhD[2-4]; Stephen Gilbert, PhD[2,6]; Valentin Meillet, MS[2-5]; Pierre Jaïs, MD, PhD[2-5]; Mélèze Hocini, MD[2-5]; Michel Haïssaguerre, MD, PhD [2-5]; Rémi Dubois, PhD[2-4]; Olivier Bernus, PhD[2-4]; Igor Efimov, PhD[1,2]

[1]Department of Biomedical Engineering, Washington University in Saint Louis, MO; [2]L'Institut de Rythmologie et Modélisation Cardiaque LIRYC, Université de Bordeaux, [3]Inserm, Centre de Recherche Cardio-Thoracique de Bordeaux U1045, [4]Université de Bordeaux, Centre de Recherche Cardio-Thoracique de Bordeaux U1045, Bordeaux, [5]CHU de Bordeaux, Hôpital du Haut Lévêque, Avenue de Magellan, Pessac, France; [6]Max Delbrück Center for Molecular Medicine, Berlin, Germany

Correspondence:

Igor Efimov, PhD

Department of Biomedical Engineering

George Washington University

800 22nd Street NW, Suite 5000

Washington, DC 20052

Tel: 202-994-1635

E-mail: efimov@gwu.edu

Journal Subject Codes: [132] Arrhythmias - basic studies, [5] Arrhythmias, clinical electrophysiology, drugs, [106] Electrophysiology

Abstract:

Background - Therapy strategies for atrial fibrillation based on electrical characterization are becoming viable personalized medicine approaches to treat a notoriously difficult disease. In light of these approaches that rely on high-density surface mapping, this study aims to evaluate the presence of three-dimensional electrical substrate variations within the transmural wall during acute episodes of atrial fibrillation.

Methods and Results - Optical signals were simultaneously acquired from the epicardial and endocardial tissue during acute fibrillation in ovine isolated left atria. Dominant frequency, regularity index, propagation angles and phase dynamics were assessed and correlated across imaging planes to gauge the synchrony of the activation patterns compared to paced rhythms. Static frequency parameters were well correlated spatially between the endocardium and the epicardium (dominant frequency, 0.79±0.06 and regularity index, 0.93±0.009). However, dynamic tracking of propagation vectors and phase singularity trajectories revealed discordant activity across the transmural wall. The absolute value of the difference in the number, spatial stability, and temporal stability of phase singularities between the epicardial and endocardial planes was significantly greater than 0 with a median difference of 1.0, 9.27%, and 19.75%, respectively. The number of wavefronts with respect to time was significantly less correlated and the difference in propagation angle was significantly larger in fibrillation compared to paced rhythms.

Conclusions - Atrial fibrillation substrates are dynamic three-dimensional structures with a range of discordance between the epicardial and endocardial tissue. The results of this study suggest that transmural propagation may play a role in AF maintenance mechanisms.

Keywords: atrial fibrillation, electrophysiology, reentry, rotor

After a century of research, atrial fibrillation (AF) remains a challenging disease to study and exceptionally resilient to treatment. Establishing a comprehensive description of AF substrates that sustain arrhythmias[1, 2] remains a formidable task. Historically, atrial tissue is assumed to be a functionally two-dimensional (2D) structure. Simulations and mapping modalities largely ignore transmural conduction during AF, emphasizing in-plane propagation patterns as the driver circuits. However, several recent animal studies have suggested that epicardial-endocardial dissociation may play an important and dynamic role in the progression of AF substrates and stability.[3-7] Although the wide diversity of the disease plays a crucial role in the mechanism controversy, it is also possible that three-dimensional (3D) conduction may account for some of the discrepancies in AF maintenance hypotheses. By taking advantage of optical tissue penetration properties, we used trans-illumination mapping to quantitatively assess the association between propagation on the epicardial and endocardial surfaces in an acute AF model compared to paced rhythms and infer the 3D heterogeneity of the substrate. Using this approach we evaluated degrees of discordance in the spatiotemporal organization of individual induced AF episodes.

Traditional optical mapping is a 2D imaging technique, transducing the electrical activity of the superficial layers of cells into optical signals that linearly depend on transmembrane potential changes[8]. However, the depth of penetration is largely based on the absorption and scattering properties of the excitation and emission light and can be tuned by wavelength and camera orientations. Simultaneous imaging at two depths within the tissue is achieved by detecting fluorescence on the ipsilateral and contralateral tissue surface relative to the illumination source.[9, 10] Additionally, near infrared voltage sensitive dyes[11] are used to increase the depth of penetration through the tissue and increase the signal to noise ratio (SNR) of the

trans-illuminated signal. The optical signals collected in the reflected and transilluminated modes are averaged signals from across depth subdivisions. Biophotonic simulations have predicted that the average depth of contribution to the reflected signal is 2.5 mm, while the average depth of the contralateral signal is 4 mm from the illuminated surface.[12] We applied this technique to correlate the simultaneous propagation patterns at two different depths within the atrial wall with high spatial resolution and without having to physically expose the transmural tissue, which may disrupt the integrity of fibrillatory circuits. For paced data we were able to look at four planes by aligning two files taken with opposing illumination. Figure 1A illustrates the two illumination configurations. For AF data the two configurations cannot be temporally aligned. In this study we used an acute acetylcholine-induced model of AF in the isolated sheep left atrium to test the hypothesis that inherent local heterogeneities in electrophysiological properties and anatomical discontinuities can support dys-synchronous electrical propagation in AF across the transmural wall independently of AF-induced structural remodeling. We used parameters that are commonly used for clinical characterization of AF including: dominant frequency, regularity index, and phase analysis. As personalized therapy strategies based on high density mapping gain favor, it is increasingly important to understand the limitations of 2D mapping techniques and the subsequent effects on the efficacy of therapy paradigms. There is no clinical technique available yet to assess transmural propagation; optical mapping provides such a platform to investigate the spatiotemporal dynamics with a finer resolution and infer transmural propagation patterns in an experimental setting.

Methods

Experimental Preparation

Optical mapping experiments were conducted in isolated left atrial (LA) preparations from Texel

crossbred sheep (N=8) weighing 40-55 kg. The animals were treated in accordance with the guidelines from Directive 2010/63/EU of the European Parliament on the protection of animals used for scientific purposes and the local Université de Bordeaux ethical committee. The sheep were pre-medicated with 20mg/kg ketamine and 0.02mL/kg acepromazine (Calmivet, France). Surgical plane anesthesia was induced with 10mg/kg sodium pentobarbital and maintained under isofluorane, 2% in 100% O_2. The chest was opened to provide access to the heart and the animal was euthanized by sodium pentobarbital (2000mg). The heart was rapidly excised and perfused with 200 mL of cardioplegia and heparin through an aortic cannula. The left coronary artery was isolated for cannulation. Under constant perfusion of cold cardioplegia the right atria was opened through the vena cava and the ventricles were removed below the main branch of the circumflex artery. All ventricular vessel branches were tied off and LA opened through the right superior pulmonary vein. The right atrium was removed and the remaining pulmonary vein ostia were inverted to maximize the exposed surface area. The LA preparation was stretched across a frame and secured to pull it flat (Figure 1). Methylene blue was applied to ensure adequate perfusion and the preparation was transferred to warm oxygenated Tyrode's solution for optical mapping. Perfusion was maintained for the duration of the experiment at 20 mL/min. The tissue was suspended vertically in a bath to allow optical access to both the endocardial and epicardial surface. Two stainless steel electrodes were clipped to the endocardial surface to record a pseudo-ECG for AF identification.

Optical Mapping Acquisition

The tissue was electromechanically uncoupled with 15μM Blebbistatin and stained with a 50μM bolus injection of di-4 ANBDQBS. The tissue was illuminated with two 660 nm LEDs (Cairn Research Ltd, Kent, UK). Fluorescence was acquired through a 715nm long pass filter using two

CMOS cameras (MICAM Ultima, SciMedia) with 5cm x 5cm fields of view (spatial resolution 500μM). The samples were paced at 2Hz from various locations with a bipolar electrode on either the epicardial and endocardial surface at 2X the pacing threshold. Four-second recordings were captured at 1,000Hz. Acetylcholine (Sigma-Aldrich, MO) was added to the perfusate in increasing concentrations from 0.1μM to 5μM until AF could be induced by 50Hz burst pacing. An AF episode was recorded if it was self-sustaining for > 30seconds.

Magnetic Resonance Imaging

Limited by equipment availability, the atria from 5 out of 8 hearts were imaged with MRI after optical mapping to obtain the complex anatomical geometry of the preparations. Immediately after the completion of the optical mapping, the perfusate was removed from the imaging chamber and replaced with YL VAC 14/6 Fomblin perfluoropolyether (Ausimont, Milan, Italy), an organofluorine with no 1H MRI signal. The sealed chamber was placed in a Siemens Magnetom Avanto 1.5T MRI scanner (Erlangen, Germany) with the axis of optical imaging aligned to the b0 direction. Imaging was carried out using a Siemens cardiac MRI sequence with a simulated ECG (cycle length 700ms), echo time 2.98ms, repetition time 399.19ms, flip angle 90°, matrix size of 512 x 512 x 192, spatial resolution of 0.62 x 0.62 x 0.31 mm^3, for a total field of view of 316 x 316 x 60 mm^3, and an acquisition time of 32 minutes. The images were segmented from the background signal using Seg3D2- 2.1.5 (Scientific Computing and Imaging Institute, University of Utah, USA). The segmentation mask was generated using a median filter and thresholding to exclude non-tissue voxels with a binary erode then dilate. The resulting segmented slices were reconstructed into a volume and further processed in Paraview using additional threshold filters and manual volume extraction to remove the ventricular tissue from the edges of the tissue preparation. Transmural thickness was estimated along a normal line

through the tissue perpendicular to the CMOS camera focal plane using a custom C++ program.

Arrhythmia Processing

All optical signals were processed with custom MATLAB software, some of which has been previously described.[13] Briefly, each pixel was spatially filtered with a 3 x 3 uniform average bin, the temporal sequences were low pass filtered by an FIR filter with a cutoff frequency of 100 Hz, drift in the baseline was removed with a polynomial fit subtraction, and the magnitude of the fluorescent change was normalized. Dominant frequency (DF) was evaluated for each pixel as the frequency band with maximal power on a periodogram calculated with a Fast-Fourier transform (resolution 0.24 Hz). Regularity index (RI) was defined as the ratio of the power within a 1 Hz band centered on the DF and the total power spectrum from 0 to 100 Hz. A perfect sine wave with a single frequency yields an RI of 1. Single parameter spatial maps were aligned using MATLAB's intensity based image registration to account for any small translation or scaling differences in camera orientation between fields of view before statistical comparisons.

Wavefront and Phase Dynamics

Prior to transforming the optical signals into the phase domain, additional levels of preconditioning were applied to both paced and AF data. The signals were temporally filtered with a narrow [2,10] Hz band pass filter and were spatially masked to keep only those pixels with SNR of at least half the maximal SNR in the field of view. SNR was calculated during a 2 Hz pacing trace for each preparation and illumination direction as the ratio of the baseline amplitude to the amplitude of an optical action potential after normalization. To convert the optical signal into the phase space we applied the Hilbert Transform on the detrended processed optical signals. Wavefronts were defined as the isophase lines along $\varphi=\frac{\pi}{2}$. The number of

discrete wavefronts was calculated for each field of view with a sampling frequency of 50Hz. Conduction velocity vectors were estimated from the direction of vectors normal to the curvature of the isophase wavefronts.[14] Conduction velocity maps were calculated with a 0.5s resolution. Phase singularities (PS) were calculated as non-zero topological charges constrained to the isophase wavefronts in each time frame. Static PS incidence maps were calculated by summing binary PS location maps across time. PS were considered distinct if they were >5 pixels apart in a single frame. The minimum Euclidean distance between PS on the two imaging planes was calculated using MATLAB's nearest neighbor search algorithm. Dynamic PS stability was calculated in terms of full wavefront rotations around the PS. Stable PS were arbitrarily defined by 2 full rotations. The spatial PS ratio is defined as the fraction of the field of view through which all stable PS track. The temporal PS ratio is the fraction of the total sequence where at least one stable PS is present.

Statistical Analysis

All means that characterize the spatial average of a single AF episode are represented as sample mean ± standard deviation. All means that characterize average Epi-Endo trends across the cohort of hearts are reported as sample mean ± standard error of the mean. When comparing transilluminated v. reflected or paced v. AF, the data points are pooled and averaged for each heart. A statistical comparison between groups is applied to the cohort of hearts with an unpaired two-tailed t-test. When the comparison was across multiple variables, i.e both fields of view and rhythm type, a multivariate analysis of variance was used. Significance was defined as $p<0.05$. When testing whether the absolute value of the difference between the endocardial and epicardial parameter is equal to 0, a one-tailed t-test is used on the average differences per heart. Mean conduction velocity vectors and angular variance are calculated from the circular distribution of

individual conduction velocity vectors from each wavefront in time.[15] The mean propagation vector is compared to the mean from the contralateral field of view for each episode. The difference in angle is averaged for each heart before a two-tailed t-test is applied between the paced and AF conditions. For comparing the wavefront count, a Pearson's linear correlation coefficient is calculated for each episode (AF and paced). The correlation coefficients are pooled and averaged within each heart, before the two groups are compared. An average 2D correlation coefficient from MATLAB is used to compare the DF and RI intensity images from each field of view in a similar manner.

Results

Two-Plane Imaging Feasibility

To verify that the dual-sided imaging technique was capturing information at two distinct depths within the tissue we calculated the breakthrough delay on the field of view contralateral to the pacing electrode, relative to the pacing spike. When the tissue was paced epicardially at 2Hz, the delay until breakthrough on the endocardial plane was 11.63±1.1ms (s.e.m) across all hearts (N=8 animals). Conversely, the delay for endocardial pacing until breakthrough on the epicardial plane was 9.6±2.52ms. SNR was calculated for both planes to further establish the feasibility of the acquisition technique. Figure 2 displays a representative distribution of SNR from both the reflected and transilluminated modes. The mean reflected SNR was 17.20 ± 1.062 (s.e.m) and the transilluminated SNR was 16.88 ± 1.062 (s.e.m) for N=8 hearts. There was no statistical difference between the two imaging acquisition modes ($p=0.84$), when assessed with a two-tailed t-test. The transilluminated signal is averaged across a greater depth, this manifests as an increase in upstroke duration, as seen in the representative optical traces in Figure 2C. The quantification of the upstroke duration distribution with each mode is shown in Supplemental Figure 1.

Transmural APD Gradients and Thickness Variation

From the MRI volumes we extracted local thickness parameters. Figure 3A shows an example volume as well as a thickness profile cut along a coronal path to highlight the complex geometric contours of the atrial tissue. Figure 3B shows the distribution of thicknesses across 5 left atrial volumes with a logarithmic normal distribution fit. Acetylcholine was added in increasing doses to each preparation, ranging from 0.1μM to 5μM, until a sustained AF was induced. Figure 3D displays the range of action potential durations (APD), Endo: 129.73±17.3 (mean ± spatial sd) to 188.19±18.51ms and Epi: 125.14±16.46 to 164.46±13.51ms during 2Hz pacing for all 8 preparations after the necessary final dose of acetylcholine was given. Representative APD maps highlight transmural differences in APD between the imaging planes (Figure 3C). For paced data the imaging acquisition protocol can create 4 distinct planes through the tissue, a reflected and trans-illuminated plane for each illumination direction that have been temporally aligned. We defined the local gradient of APD as the difference from the reflected signals during endocardial illumination, to the reflected signals from epicardial illumination. The average transmural gradient in APD from endocardium to epicardium was ΔAPD=24.13±6.24ms (N=8). Finally, we registered the thickness map to the transmural APD gradient plane (Figure 3E). Although both the thickness and the APD transmural differences were heterogeneously dispersed across the field of view there was no correlation between these two parameters.

Arrhythmia Static Parameters

A total of 10 epicardially-illuminated episodes and 10 endocardially-illuminated episodes were included in the analysis. The mean DF and spatial standard deviation, including both the endocardial and epicardial field of view, ranged from 3.90±0.48 to 10.03±2.88 Hz. The difference between epicardial and endocardial global DF was not significantly different from

zero when assessed by a two-tailed t-test (p=0.3516, N=8 hearts). The global mean RI and spatial standard deviation ranged from 0.12±0.065 to 0.704 ± 0.079, with an Epi-Endo difference that was not significantly greater than zero (p=0.42, N=8 hearts). The distributions in the Epi-Endo difference of these global parameters across all hearts are shown in Figure 4A. Two representative examples are displayed in Figure 4B, highlighting the visual resemblance across both the imaging planes. The spatial distribution of DF across the transmural wall had an average 2D correlation across all hearts of 0.79±0.06 (s.e.m). Likewise, the spatial distribution of the RI had an average correlation of 0.930±0.009, with no statistical difference between illumination configurations (Figure 4C). PS incidence maps were created as a static characterization of each arrhythmia. Two PS incidence maps are shown in Supplementary Figure 2. The mean distance between the static PS locations and the nearest PS on the contralateral side was 5.24±0.3mm (N=8).

Arrhythmia Dynamics

All dynamic parameters are presented in comparison to paced data as a control to account for the effect of anatomical complexities on the optical planes and SNR edge effects on the fields on view. The dynamic number of propagation wavefronts was quantified in a time series and correlated with the opposing side (Figure 5). Figure 5A-B illustrates the wavefront identification and displays representative wavefront count traces for a paced rhythm and an AF episode (Figure 5A-B). The mean correlation between epicardial and endocardial wavefront count was 0.69±0.035 for pacing versus 0.47±0.048 for AF (p=0.0028, two-tailed t-test, N=8 hearts). The average direction of propagation was calculated for each episode with a resolution of 0.5s with a random starting time. A representative propagation angle calculation from both the paced and AF groups is shown in Figure 6A-B along with the angular distribution. The statistically significant

(p=0.044, N=8 hearts) difference in angle between the two planes was 20.37±3.04° during pacing and 61.43±12.37° during AF (Figure 6C). A one-way multivariate analysis of variance confirmed that the angular variance did not differ between rhythms or fields of view.

The PS dynamics are specific to each heart and even vary between separate AF episodes within a single preparation. Therefore, we report the detailed observations of two AF episodes and the summary of phase tracking for the remainder of the episodes (Figure 7). Table 1 quantitatively describes two individual episodes, representing two types of complexity and transmural dynamics: the first is less complex but has discordant phase dynamics across the two imaging planes while the second is more complex but displays more conserved dynamics across the transmural wall. Sample optical traces from corresponding pixels in both fields of view and electrical bath traces for each example AF episode are displayed in Supplemental Figure 3. AF episode 1 shows a temporally stable epicardial rotor with minimal spatial meandering, while the dynamics at the endocardium are less stable in both the temporal and spatial domain. The pattern can be visualized in a dynamic phase map (Video 1) as well as the dynamic potential map (Video 2). This dyssynchrony manifests in an increase in the PS count with less rotations on the endocardium, while the constant driver is veiled in this imaging plane (Figure 7A). In contrast, in AF episode 2, the spatial and temporal trajectories of one imaging plane nearly trace the trajectories from the opposing plane (Figure 7B), which is reflected in similar spatial and temporal ratios. The dynamic conservation of propagation pattern is emulated in the small difference observed between propagation vectors (Table 1) and visualized in Videos 3-4.

Figure 7C extends these observations to all hearts. The correlation coefficient between the number of PS on the endocardial imaging plane and the PS count on the epicardial plane is 0.879. The average number of stable PS was 4.04±0.66 (s.e.m, N=8 hearts) and 3.3±0.59 for the

endo and epi plane respectively. The absolute value of the difference in PS count between the epicardial and endocardial plane was significantly greater than 0 with a median difference of 1.0 PS ($p=1.01x10^{-5}$, 1 tailed t-test). The correlation coefficient across all hearts for the spatial stability ratio is 0.795. The average area across all hearts through which stable PS trajectories traversed was 4.63±1.05 cm^2 (endo) and 3.56±1.0 cm^2 (epi). The absolute value of the difference between the epicardial and endocardial plane was significantly greater than 0 with a median difference of 9.27% ($p=5.87x10^{-4}$, N=8 hearts). The correlation coefficient for the ratio of time that has at least one stable PS present between the imaging planes is 0..111 across all hearts. The absolute value of the difference between the epicardial and endocardial plane was significantly greater than 0 with a median difference of 19.75% ($p=2.78x10^{-4}$, N=8 hearts).

Discussion

Modern clinical mapping techniques are confined to observing only the surface manifestations of 3D propagation patterns. In a manuscript describing the 3D organizing centers of chemical waves, which are analogous to propagation in excitable media, Winfree recognized that although a pattern could be discerned within a 2D plane, it would be nearly impossible to identify the organizing center without the complete 3D perspective.[16] Several reports have suggested that AF organizing centers may also be more completely described as 3D structures. A substantial 3D component of AF drivers could contribute to the complexity of personalized therapy approaches.

Dyssynchronous transmural activation was documented with simultaneous endocardial and epicardial recordings as early as 1993.[17] Using unipolar electrode recordings, Schuessler et al. correlated discordant activation activity with anatomic heterogeneities of the canine right atrium in acute AF. Importantly, neither surface was preferentially faster during tachyarrhythmia propagation. A recent *in vivo* mapping study by Eckstein et al. quantified the percentage of

fibrillation waves that were preceded by electrical activity on the contralateral surface.[4] The authors reported a marked increase in the incidence of breakthrough with an increase in the degree of epi-endo dissociation, suggesting that what may appear to be a focal source is actually due to 3D transmural propagation. Yamazaki et al. used simultaneous epicardial and localized endoscopically-guided endocardial optical mapping to predict the virtual transmural architecture of rotors.[6] The presented results show some rotors in phase on both planes and some with a filament twist or non-identical activation patterns. In their study the rotors were often associated with sharp transitions in tissue thickness and the thinnest regions.

Several studies have investigated more sustained effects of transmural differences on the progression of AF. One such study, conducted by Everett et al, performed endocardial noncontact mapping and epicardial plaque electrode mapping in 5 different models of AF in canines to assess the effect of structural remodeling on the dimensionality of the AF substrate.[5] The authors found that models with only electrical remodeling showed more dissimilarity between the endocardial and epicardial surface activation patterns than models that also incorporated structural remodeling. Conversely, Eckstein et al charted the time course of epi-endo dissociation during pacing-induced AF in goats and suggested that progressive uncoupling in both the longitudinal and the transmural dimension promote stability of AF.[18] The study also suggests that greater degrees of dissociation occur in the thicker atrial tissue. Computationally, a dual layer simulation by Gharaviri et al suggested that epi-endo dyssynchrony increased AF stability compared to single layer simulations.[19] The model was only a proof of principle simulation with arbitrarily placed discrete transmural connections. Even so, the incorporation of a third dimension for propagation increased the number of wavefronts at any given time and the lifespan of phase singularities without effecting the frequency content of the simulated

arrhythmia, in agreement with the data observed in our study.

Our study continues the line of work towards 3D AF substrate characterization by charting the dynamic dissociation between layers and probing the transmural uniformity of potential drivers with expanded spatial coverage and resolution. The global DF and the spatial distribution of DF are both well conserved across the transmural wall. The RI is also well conserved as a global mean and a spatial pattern. However, the frequency content does not represent a complete characterization of the dynamic AF substrate. In order to further assess the transmural uniformity of the substrate we investigated individual wavefront dynamics. Compared to paced rhythms, the dynamic wavefront count is less correlated during an arrhythmia. The observed correlation for paced rhythms is not 1 as might be expected. The observed value may be due to the SNR spatial mask partitioning a single wavefront into multiple segments on one imaging plane as seen in Figure 5A. It may also be the result of breakthrough delay on the side contralateral to the pacing electrode. This unexpected outcome illustrates why we used the pacing data as a control instead of analyzing the AF episodes in isolation. We also evaluated the difference in shape of the propagating wavefront from each imaging plane, through propagation vector angles. The pacing wavefronts move in unison across the tissue, except immediately following the pacing spike (not shown in figure). However, the propagation during the arrhythmia is significantly less uniform across the transmural wall with a significantly greater difference in mean propagation angle. Figure 6B shows a representative example of an endocardial wavefront that is trailing behind the simultaneous epicardial pattern. The mean difference in angle shows that the organizing centers of the AF substrate have 3D components, resulting in a difference in the propagation vector direction.

Phase plane analysis is a technique derived from the physics of vortices (e.g. spiral

waves, rotors, scrolls, etc.) and applied as a popular method to map the organizing centers of the AF substrates.[20-25] Although the algorithms employed vary between institutions with various degrees of clinical efficacy, the theory behind PS tracking is sound and well established. The conversion from potential space into phase space assigns a unique value to each instant of time within one period of a signal, which can be dynamic in fibrillation. Spatially, a PS forms at the wavebreak of reentry or wavefronts collisions.. These singularity points can be localized and tracked through time as a dynamic indicator of the spatiotemporal organization and stability of an AF episode. In this study we used simultaneous endocardial and epicardial mapping to investigate the contralateral activity at the site of stable PS to assess the transmural uniformity of the dynamic AF substrate. PS incidence maps show that the distance to the nearest neighboring PS on the contralateral surface is relatively small suggesting that PS are macroscopically localized to similar regions of the left atrium. In fact the distance seems to be similar in size to an ablation catheter tip, which may explain why driver ablation has seen some success. However, due to tissue curvature, this observation does not allow to directly infer the transmurality of the rotor. For example, if tissue is curved and the rotor filament is perpendicular to the tissue surface (no transmural variations in rotor properties) then the PS will appear displaced with respect to each other in the imaging planes. Conversely, a more complex intramural filament may give rise to what would seem like perfectly aligned PS on epi and endo imaging planes. Additionally the locations with the highest relative frequency of a PS assume each time frame is independent, which puts greater emphasis on the PS with less spatial meandering that repeatedly pass through the same pixel often. Therefore the PS trajectories may be a more important spatial measure of the transmural synchrony of organizing centers than the PS incidence maps.

Consequently, we simultaneously mapped the PS trajectories of stable PS, defined as

when the wavefront passes 2 full rotations or 4π around the singularity, in both the epicardial and the endocardial imaging planes. We used the spatial ratio and the time ratio as measures of the colocalization across the transmural wall in the spatial and temporal domains. Although all three parameters we tested showed differences across the wall significantly greater than zero, the greatest measure of discordance was found in the temporal stability of PS across surfaces. The spatial meandering and PS count are more conserved on average, although episode 1 does display a greater degree of meandering preferential to the endocardial plane. AF Episode 1 demonstrates how non-uniform transmural propagation leads to breakthrough that disrupts the stable organized propagation pattern. The propagation videos show that the endocardial wavebreak does not occur on every pass of the stable rotation but does repeat several times within the sequence. The traces in Supplemental Figure 3 also show propagation in the endocardial plane that is near-continuously out of phase with the epicardial trace. Detailed episode 2 is an example of an AF substrate that is more uniform across the transmural wall. Although not always completely synchronous, the PS track together through time and space. The video displays an obviously synchronous collective pattern. The traces in Supplemental Figure 3 echo this pattern; there are short bursts of out of phase propagation (e.g. 1000-1500ms) but the traces track in sync for the majority of the measured sequence. The cohort of AF episodes included in this study lies along a spectrum of transmural uniformity outlined by these two examples. However, there was no correlation between frequency content and degree of dissociation that could help predict which episodes are likely to exhibit transmural differences (data not shown). There were fast and slow, disorganized and regular, single rotor and many PS arrhythmias that had varying levels of functional dissociation. A single surface manifestation of these episodes would not have captured the complete view of the dynamic 3D substrates in this

study.

The acute model of AF does not incorporate pathophysiological structural remodeling, which could conceivably compound the degree of dyssynchrony observed across the transmural wall. In this model the likely sources of transmural dyssynchrony are abrupt changes in geometrical thickness due to complex contours of the atrium including the pulmonary vein ostia, trabeculations and appendage or a heterogeneous response to acetylcholine. Each heart did display regional differences in APD after acetylcholine, creating transmural dissimilarities. However, there was no correlation between the transmural repolarization gradient and thickness, nor was there a correlation with the APD differences across the wall and the spatial pattern of the frequency content (Supplemental Figure 4). It is possible that dyssynchrony locates at the interface between these two factors, where there is substantial space anatomically and a considerable gap between repolarization to harbor transmural conduction. This study does not rigorously identify the tissue conditions that are favorable to discordant propagation patterns, instead focusing on chronicling the spatiotemporal prevalence of dissociated patterns. Future work would require transmural discontinuities to be assessed histologically to obtain further insight into the source of dyssynchrony.

Limitations

AF is an exceptionally diverse disease. We used a range of acetylcholine doses to encompass the variability of clinical AF with respect to frequency content and organization in this study. Still, there are some limitations to extending this model to the clinical population of AF. Most notably, this is not a model that is favorable to automaticity. The depression of focal discharges by acetylcholine[26] creates a substrate that fosters re-entry and rotor drivers. Additionally, although the image acquisition technique allows for multiple planes to be imaged simultaneously, it is still

not possible to fully capture out of plane rotation. The biophotonic simulations provide an estimate for the depth of the contributing signal for each illumination/optical configuration; however, in practice there are many variables that could affect this parameter including: the angle of incidence of light, the focal plane of the cameras, and the complex contours of the anatomy. We used the pacing data as a control to account for some of these effects that vary from experiment to experiment.

Conclusions

The results of this study, along with recent literature, confirm that AF propagation is a 3D phenomenon with a range of transmural discordance. Although global parameters like dominant frequency and regularity index are well conserved across the transmural wall, dissociation and the role of transmural conductance are exposed with a spatiotemporal characterization of wavefront and PS dynamics in an acute model of AF that was mostly driven by short-lived meandering rotors.

Funding Sources: This work was supported by the Agence Nationale de la Recherche grant number ANR-10-IAHU04-LIRYC and under the ANR Programme Blanc (TEMPO), the Marie Curie Intra-European Fellowship program (IEF-PSCD and IEF-MSIA), the European Union Seventh Framework Programme (FP7/2007-2013) under grant agreement n° 261057 (EUTRAF), the Whitaker International Summer Grant, and the National Institutes of Health grants R01 HL115415 and R43 HL114329.

Conflict of Interest Disclosures: Igor Efimov is a stock holder and a member of the board of directors at Cardialen, Inc. Pierre Jais, Mélèze Hocini, Michel Haïssaguerre, and Rémi Dubois are stock holders in CardioInsight, Inc. Rémi Dubois is a paid consultant for CardioInsight, Inc. The other authors report no conflicts.

References:

1. Efimov IR, Gutbrod S. "Fibrillating atrium: Rabbit warren! Not beehive!". *J Cardiovasc Electrophysiol*. 2013;24:336-337.

2. Nattel S. New ideas about atrial fibrillation 50 years on. *Nature*. 2002;415:219-226.

3. Eckstein J, Schotten U. Rotors and breakthroughs as three-dimensional perpetuators of atrial fibrillation. *Cardiovasc Res*. 2012;94:8-9.

4. Eckstein J, Zeemering S, Linz D, Maesen B, Verheule S, van Hunnik A, Crijns H, Allessie MA, Schotten U. Transmural conduction is the predominant mechanism of breakthrough during atrial fibrillation: Evidence from simultaneous endo-epicardial high-density activation mapping. *Circ Arrhythm Electrophysiol*. 2013;6:334-341.

5. Everett TH, Wilson EE, Hulley GS, Olgin JE. Transmural characteristics of atrial fibrillation in canine models of structural and electrical atrial remodeling assessed by simultaneous epicardial and endocardial mapping. *Heart rhythm*. 2010;7:506-517.

6. Yamazaki M, Mironov S, Taravant C, Brec J, Vaquero LM, Bandaru K, Avula UM, Honjo H, Kodama I, Berenfeld O, Kalifa J. Heterogeneous atrial wall thickness and stretch promote scroll waves anchoring during atrial fibrillation. *Cardiovasc Res*. 2012;94:48-57.

7. Berenfeld O, Yamazaki M, Filgueiras-Rama D, Kalifa J. Surface and intramural reentrant patterns during atrial fibrillation in the sheep. *Methods Inf Med*. 2014;53.

8. Bray MA, Wikswo JP. Examination of optical depth effects on fluorescence imaging of cardiac propagation. *Biophys J*. 2003;85:4134-4145.

9. Baxter WT, Mironov SF, Zaitsev AV, Jalife J, Pertsov AM. Visualizing excitation waves inside cardiac muscle using transillumination. *Biophys J*. 2001;80:516-530.

10. Caldwell BJ, Wellner M, Mitrea BG, Pertsov AM, Zemlin CW. Probing field-induced tissue polarization using transillumination fluorescent imaging. *Biophys J*. 2010;99:2058-2066.

11. Matiukas A, Mitrea BG, Qin M, Pertsov AM, Shvedko AG, Warren MD, Zaitsev AV, Wuskell JP, Wei MD, Watras J, Loew LM. Near-infrared voltage-sensitive fluorescent dyes optimized for optical mapping in blood-perfused myocardium. *Heart Rhythm*. 2007;4:1441-1451.

12. Walton R, Bernus O. Dual excitation wavelength optical imaging of transmural electrophysiological heterogeneity in pig ventricles. *J Electrocardiol.* 2013;46:e35.

13. Laughner JI, Ng FS, Sulkin MS, Arthur RM, Efimov IR. Processing and analysis of cardiac optical mapping data obtained with potentiometric dyes. *Am J Physiol Heart Circ Physiol.* 2012;303:H753-765.

14. Kay MW, Gray RA. Measuring curvature and velocity vector fields for waves of cardiac excitation in 2-d media. *IEEE Trans Biomed Eng*. 2005;52:50-63.

15. Zar JH. *Biostatistical analysis, 5th ed.* . New Jersy, USA: Pearson Education, Inc; 2010.

16. Winfree AT, Caudle S, Chen G, McGuire P, Szilagyi Z. Quantitative optical tomography of chemical waves and their organizing centers. *Chaos*. 1996;6:617-626.

17. Schuessler RB, Kawamoto T, Hand DE, Mitsuno M, Bromberg BI, Cox JL, Boineau JP. Simultaneous epicardial and endocardial activation sequence mapping in the isolated canine right atrium. *Circulation*. 1993;88:250-263.

18. Eckstein J, Maesen B, Linz D, Zeemering S, van Hunnik A, Verheule S, Allessie M, Schotten U. Time course and mechanisms of endo-epicardial electrical dissociation during atrial fibrillation in the goat. *Cardiovasc Res*. 2011;89:816-824.

19. Gharaviri A, Verheule S, Eckstein J, Potse M, Kuijpers NH, Schotten U. A computer model of endo-epicardial electrical dissociation and transmural conduction during atrial fibrillation. *Europace.* 2012;14 Suppl 5:v10-v16.

20. Gray RA, Pertsov AM, Jalife J. Spatial and temporal organization during cardiac fibrillation. *Nature*. 1998;392:75-78.

21. Haissaguerre M, Hocini M, Shah AJ, Derval N, Sacher F, Jais P, Dubois R. Noninvasive panoramic mapping of human atrial fibrillation mechanisms: A feasibility report. *J Cardiovasc Electrophysiol*. 2013;24:711-717.

22. Rogers JM. Combined phase singularity and wavefront analysis for optical maps of ventricular fibrillation. *IEEE Trans Biomed Eng.* 2004;51:56-65.

23. Krinsky V, Efimov I. Vortices with linear cores in mathematical models of excitable media. *Physica*. 1992;188A:55-60.

24. Fast VG, Efimov I. Stability of vortex rotation in an excitable cellular medium. *Physica*. 1991;49D:77-81.

25. Haissaguerre M, Hocini M, Denis A, Shah AJ, Komatsu Y, Yamashita S, Daly M, Amraoui S, Zellerhoff S, Picat MQ, Quotb A, Jesel L, Lim H, Ploux S, Bordachar P, Attuel G, Meillet V, Ritter P, Derval N, Sacher F, Bernus O, Cochet H, Jais P, Dubois R. Driver domains in persistent atrial fibrillation. *Circulation*. 2014;130:530-538.

26. de Carvalho AP, Hoffman BF, de Carvalho MP. Two components of the cardiac action potential. I. Voltage-time course and the effect of acetylcholine on atrial and nodal cells of the rabbit heart. *J Gen Physiol*. 1969;54:607-635.

Table 1: Detailed Dynamic Analysis of Two AF Episodes. DF/RI values represented by spatial mean +/- spatial s.d, PS rotations values represented by sample mean +/- s.e.m, and propagation angle represents angular mean +/- angular variance. FOV, field of view. DF, dominant frequency, RI, regularity index, PS, phase singularity.

AF* Episode	FOV†	DF‡	RI§	Stable PS‖ Count	PS Rotations	Wavefront Count Correlation	Propagation Angle (degrees)	PS Spatial Ratio	PS Time Ratio
1	Endo	4.50±1.46	0.39±0.18	3	2.62±0.27	0.2815	230.47±59.95	0.102	0.311
	Epi	4.79±1.58	0.44±0.15	1	26.02±0		305.24±14.23	0.011	0.995
2	Endo	7.78±1.78	0.19±0.09	9	2.97±0.23	0.3608	179.44±27.5	0.085	0.882
	Epi	8.88±1.64	0.18±0.07	5	4.6±0.8		176.37±31.89	0.084	0.899

*Atrial Fibrillation, † Field of View, ‡ Dominant Frequency, § Regularity Index, || Phase Singularity.

Figure Legends:

Figure 1: Experimental Set-Up: **A**: Schematic representation of the acquisition technique. I) Endocardially illuminationed configuration with a reflected endocardial signal and a transilluminated epicardial signal. II) Epicardially illuminated configuration with a reflected epicardial signal and a transilluminated endocardial signal**. B:** Schematic representation of the two simultaneous planes captured during configuration I and example optical action potential traces from each plane. **C:** A representative tissue preparation of the left atrium showing both fields of view (white boxes).

Figure 2: Signal Morphology and Signal Quality: **A:** Spatial signal to noise ratio (SNR) maps confirming a large field of view from both simultaneous planes. **B:** Representative optical mapping traces showing the difference in upstroke morphology of the transilluminated signals. Right: magnified view of upstroke to highlight slope differences.

Figure 3: Transmural Heterogeneities: **A:** A representative volume reconstructed from the MR images, colored by depth. The trace shows the thickness along the plane in the volume to highlight the contours of the atria. **B:** Histogram showing the distribution of depths across 5 hearts with a lognormal distribution fit. **C:** Representative distribution of APD after acetylcholine **D:** Correlation between endocardial and epicardial APD after acetylcholine (Red error bars represent s.d. in the endocardial field of view, Blue error bars represent s.d. in the epicardial field of view). **E:** Example correlation between APD gradient and registered thickness map.

Figure 4: Global AF Characterization: **A:** Differences in global dominant frequency and regularity index across all hearts. **B:** Representative spatial maps of dominant frequency and regularity index for a two episodes of AF. **B:** Summary of spatial correlation between imaging plane for both parameters. Error bars represent s.e.m.

Figure 5: Transmural Correlation for Wavefront Count: **A-B:** Representative example of wavefront identification with optical mapping traces and corresponding temporal sequences of wavefront count for a paced rhythm **(A)** and a fibrillatory rhythm **(B)**. **C:** Summary of the transmural correlation of the wavefront count across imaging planes. Error bars represent s.e.m. Difference is statistically significant between the pacing and AF when both illumination directions are combined.

Figure 6: Angle of Propagation across the Transmural Wall. **A** (pacing)**-B** (AF)**:** Representative propagation vector angle distributions**. I)** Simultaneous phase maps from endo and epi fields of view with wavefronts highlighted in white, curvature arrows are displayed along the wavefronts. **II)** Circular histograms of propagation vectors for endo (blue) and epi (red) fields of view. **III)** Average angle calculations for endo (blue) and epi (red). **C:** Summary of average angle differences. Error bars represent s.e.m. Statistically significant difference observed between pacing and AF.

Figure 7: Phase Singularity Dynamics: **A** (AF Episode 1) **– B** (AF Episode 2)**: I)** Representative phase maps with wavefronts highlighted in white. II) Spatial trajectories of all PS superimposed

on the optical field of view images for endo (blue) and epi (red) imaging planes. III) Simultaneous PS trajectories in spatiotemporal domain for endo (blue) and epi (red) imaging planes. C) Summary of PS correlation data across all 20 AF episodes including PS count, spatial ratio, and temporal ratio. AF Episode 1(green).AF Episode 2 points (pink).

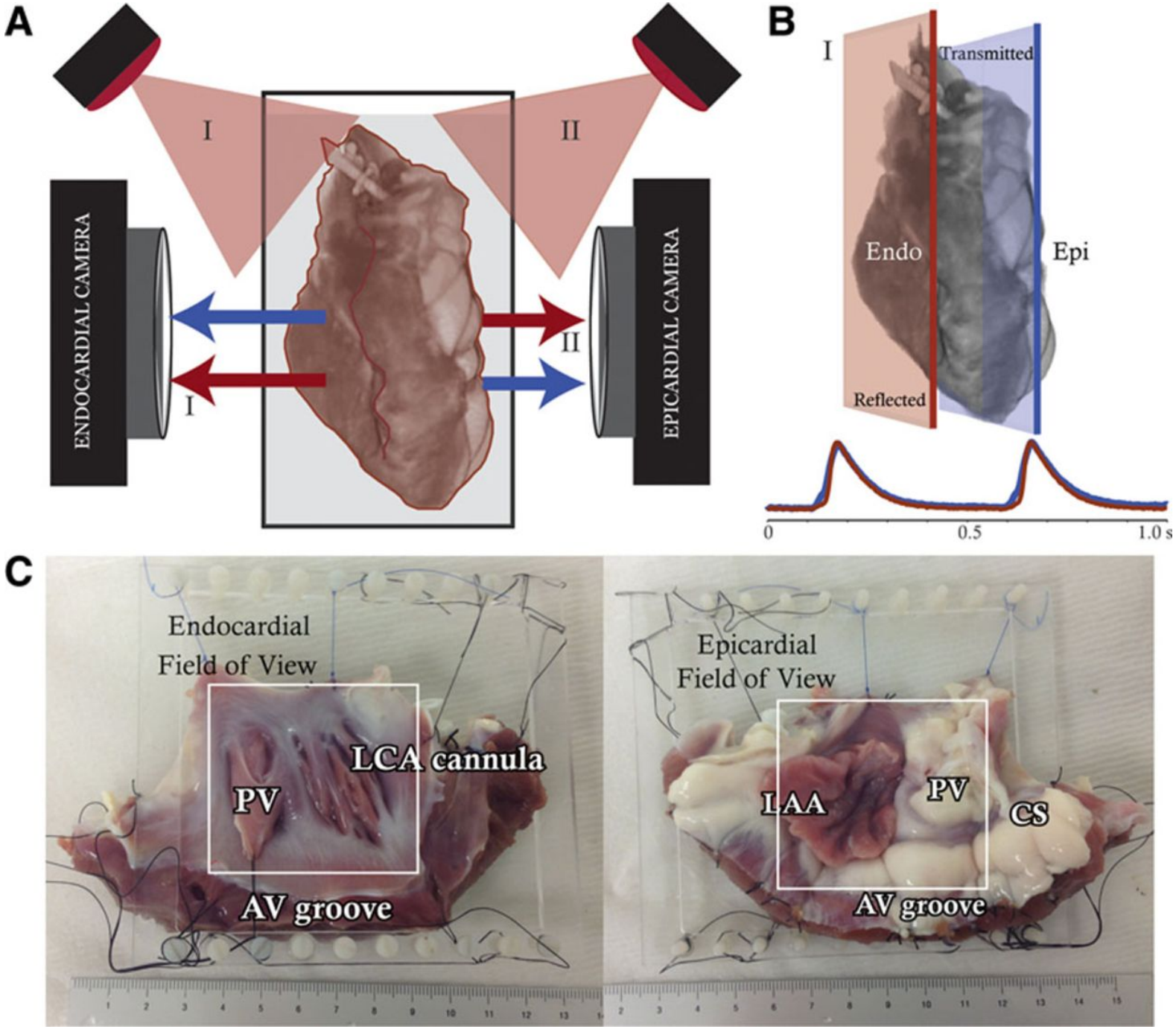
A
I
II
ENDOCARDIAL CAMERA
EPICARDIAL CAMERA
I
II
B
I
Transmitted
Endo
Epi
Reflected
0
0.5
1.0 s
C
Endocardial
Field of View
LCA cannula
PV
AV groove
Epicardial
Field of View
LAA
PV
CS
AV groove

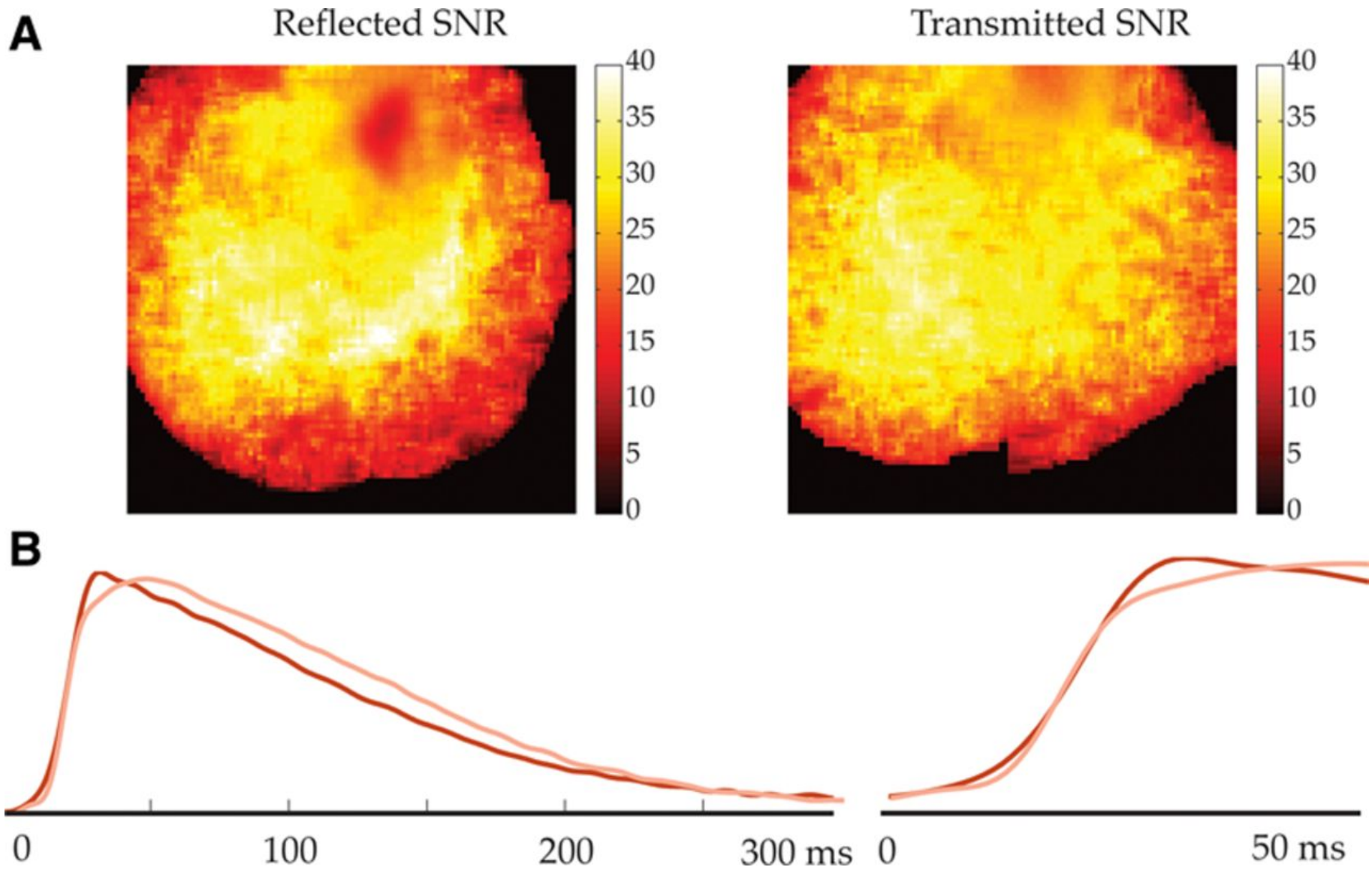
A
Reflected SNR
Transmitted SNR
40
35
30
25
20
15
10
5
0
B
0
100
200
300 ms
0
50 ms

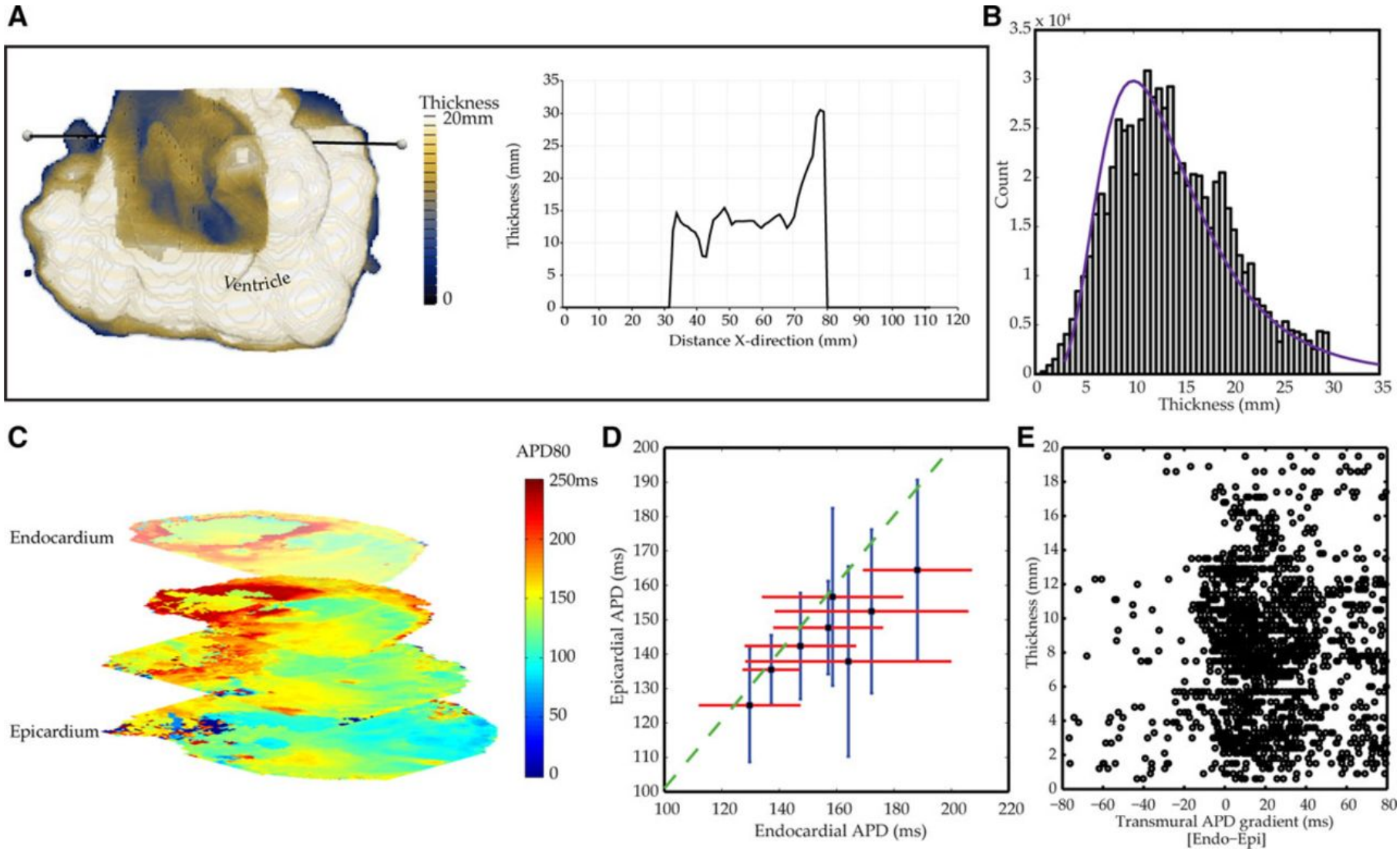
A
Thickness
20mm
0
Ventricle
Thickness (mm)
Distance X-direction (mm)
B
x 10^4
Count
Thickness (mm)
C
APD80
250ms
200
150
100
50
0
Endocardium
Epicardium
D
Epicardial APD (ms)
Endocardial APD (ms)
E
Thickness (mm)
Transmural APD gradient (ms)
[Endo−Epi]

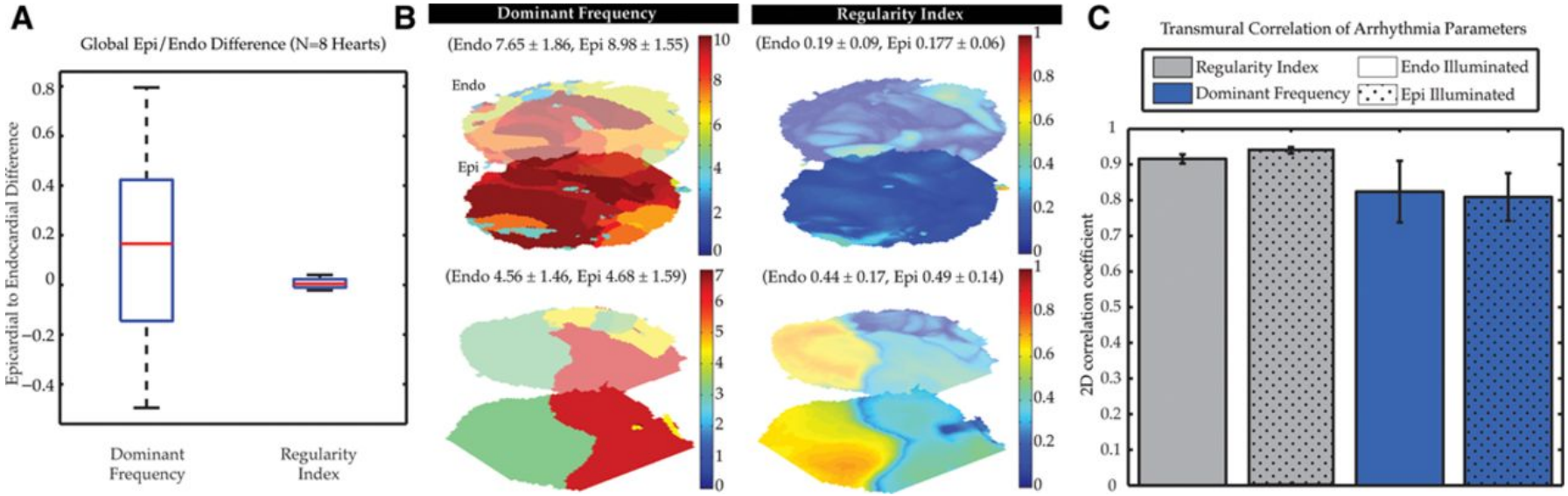
A
Global Epi/Endo Difference (N=8 Hearts)
Epicardial to Endocardial Difference
0.8
0.6
0.4
0.2
0
−0.2
−0.4
Dominant Frequency
Regularity Index
B
Dominant Frequency
Regularity Index
(Endo 7.65 ± 1.86, Epi 8.98 ± 1.55)
(Endo 0.19 ± 0.09, Epi 0.177 ± 0.06)
Endo
Epi
10
8
6
4
2
0
1
0.8
0.6
0.4
0.2
0
(Endo 4.56 ± 1.46, Epi 4.68 ± 1.59)
(Endo 0.44 ± 0.17, Epi 0.49 ± 0.14)
7
6
5
4
3
2
1
0
C
Transmural Correlation of Arrhythmia Parameters
Regularity Index
Dominant Frequency
Endo Illuminated
Epi Illuminated
2D correlation coefficient
1
0.9
0.8
0.7
0.6
0.5
0.4
0.3
0.2
0.1
0

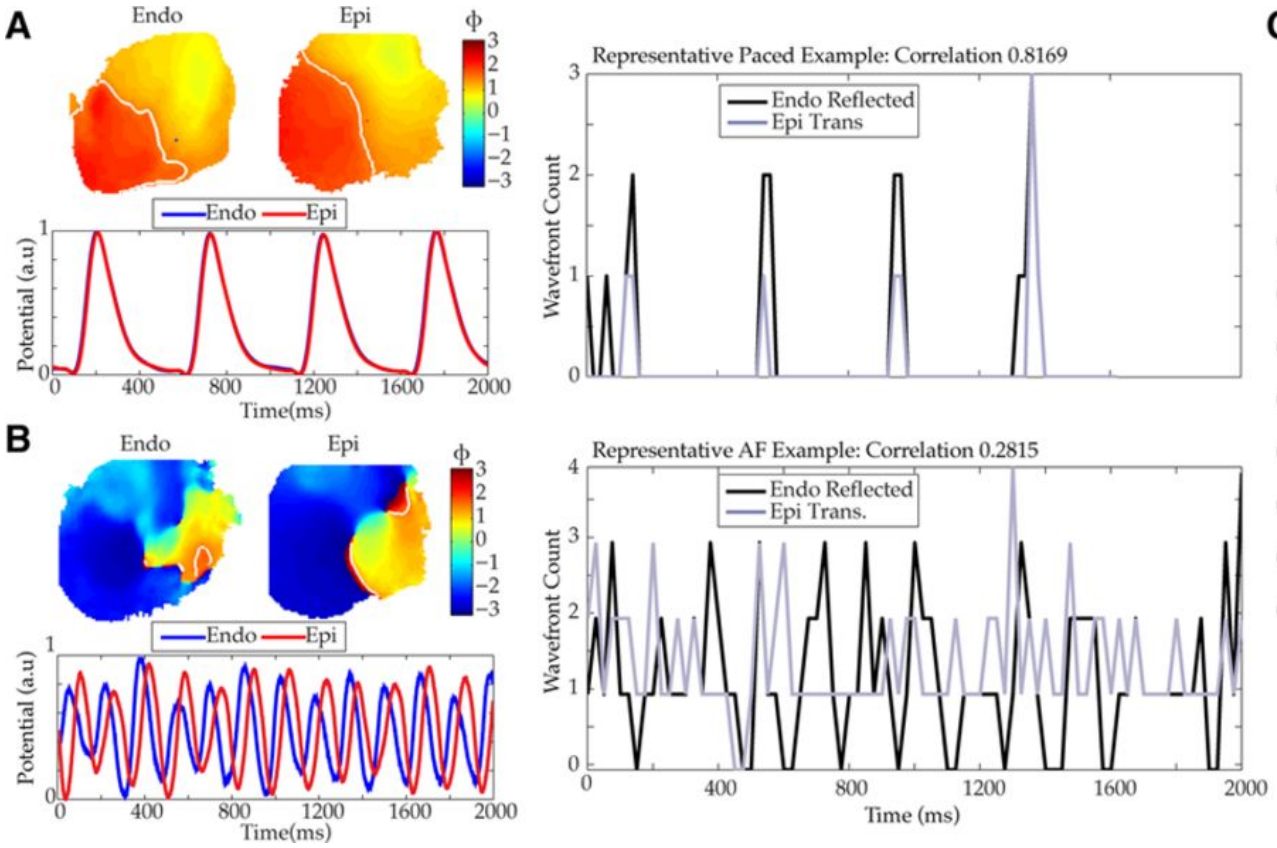
A
Endo
Epi
ϕ
3
2
1
0
−1
−2
−3
Endo
Epi
Potential (a.u)
1
0
0
400
800
1200
1600
2000
Time(ms)
B
Endo
Epi
ϕ
Endo
Epi
Potential (a.u)
Time(ms)
Representative Paced Example: Correlation 0.8169
Endo Reflected
Epi Trans
Wavefront Count
Representative AF Example: Correlation 0.2815
Endo Reflected
Epi Trans.
Wavefront Count
Time (ms)
C
Transmural Correlation of Activation Wavefronts in Time Domain
p=0.0028
0
0.1
0.2
0.3
0.4
0.5
0.6
0.7
0.8
0.9
Paced Rhythm (2Hz)
Atrial Fibrillation
Endo Illuminated
Epi Illuminated

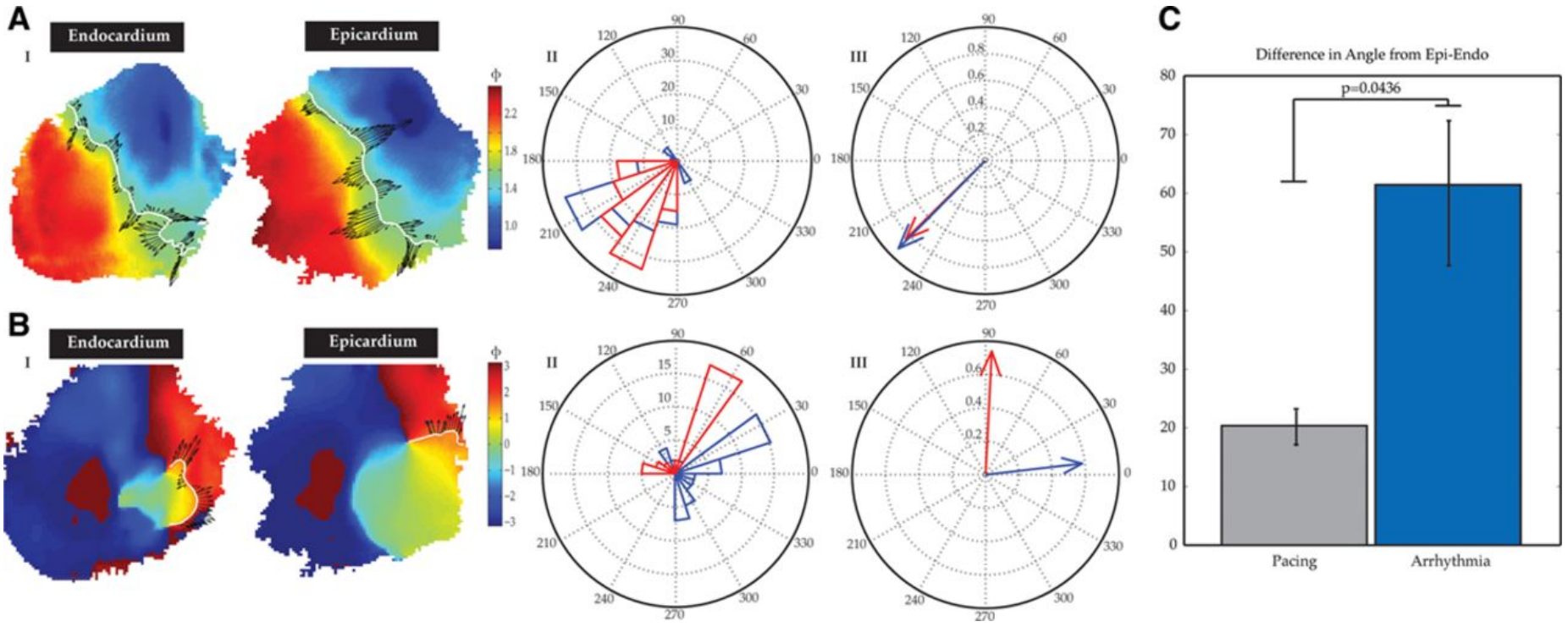
A
Endocardium
Epicardium
I
ϕ
2.2
1.8
1.4
1.0
II
III
B
Endocardium
Epicardium
I
ϕ
3
2
1
0
−1
−2
−3
II
III
C
Difference in Angle from Epi-Endo
p=0.0436
Pacing
Arrhythmia

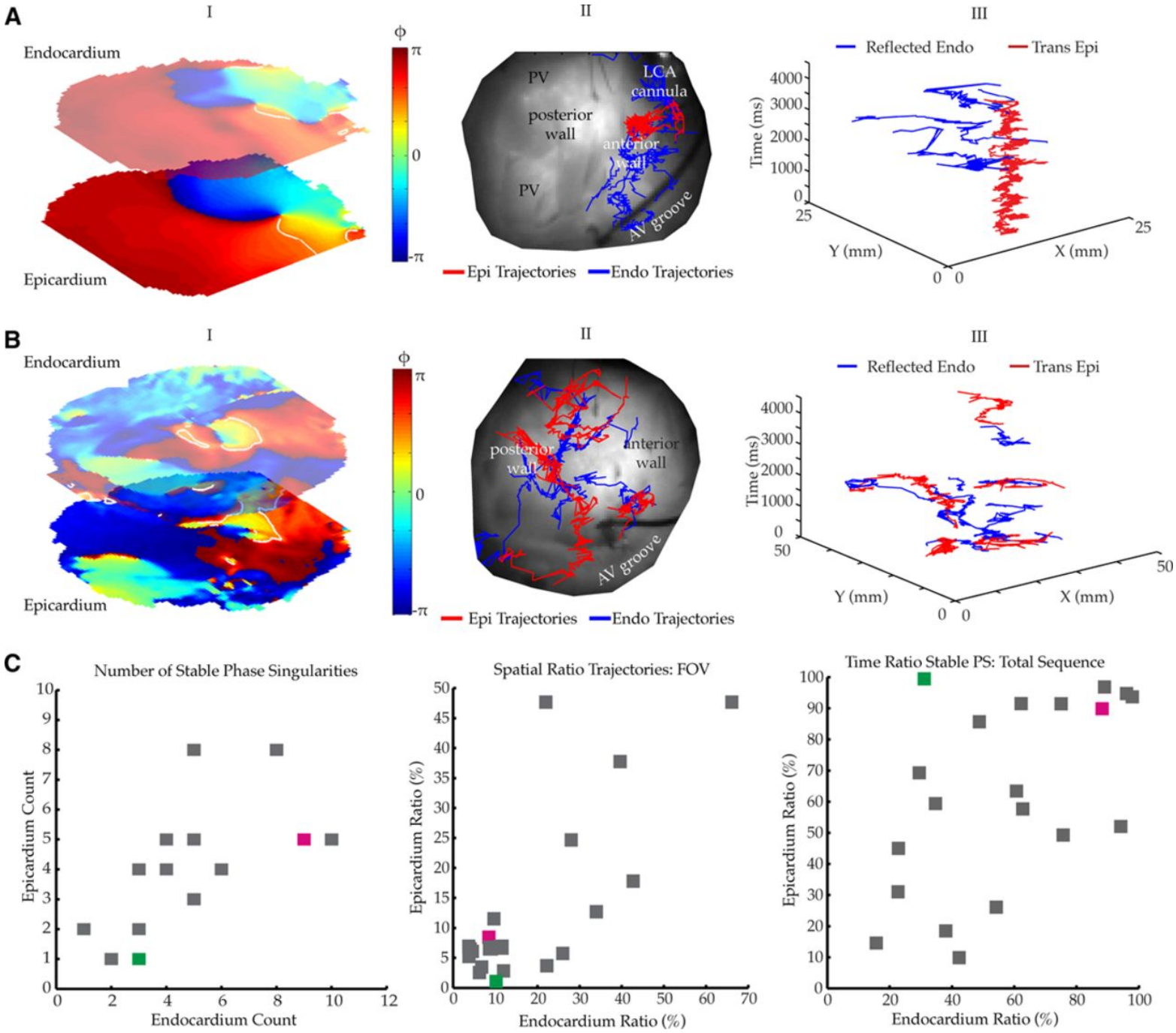
A
I
II
III
Endocardium
Epicardium
ϕ
π
0
-π
PV
LCA cannula
posterior wall
anterior wall
PV
AV groove
Epi Trajectories
Endo Trajectories
Reflected Endo
Trans Epi
Time (ms)
4000
3000
2000
1000
0
25
Y (mm)
0
0
X (mm)
25
B
I
II
III
Endocardium
Epicardium
ϕ
π
0
-π
posterior wall
anterior wall
AV groove
Epi Trajectories
Endo Trajectories
Reflected Endo
Trans Epi
Time (ms)
4000
3000
2000
1000
0
50
Y (mm)
0
0
X (mm)
50
C
Number of Stable Phase Singularities
Epicardium Count
Endocardium Count
Spatial Ratio Trajectories: FOV
Epicardium Ratio (%)
Endocardium Ratio (%)
Time Ratio Stable PS: Total Sequence
Epicardium Ratio (%)
Endocardium Ratio (%)

Supplemental Material

Figures:

Supplemental Figure 1:

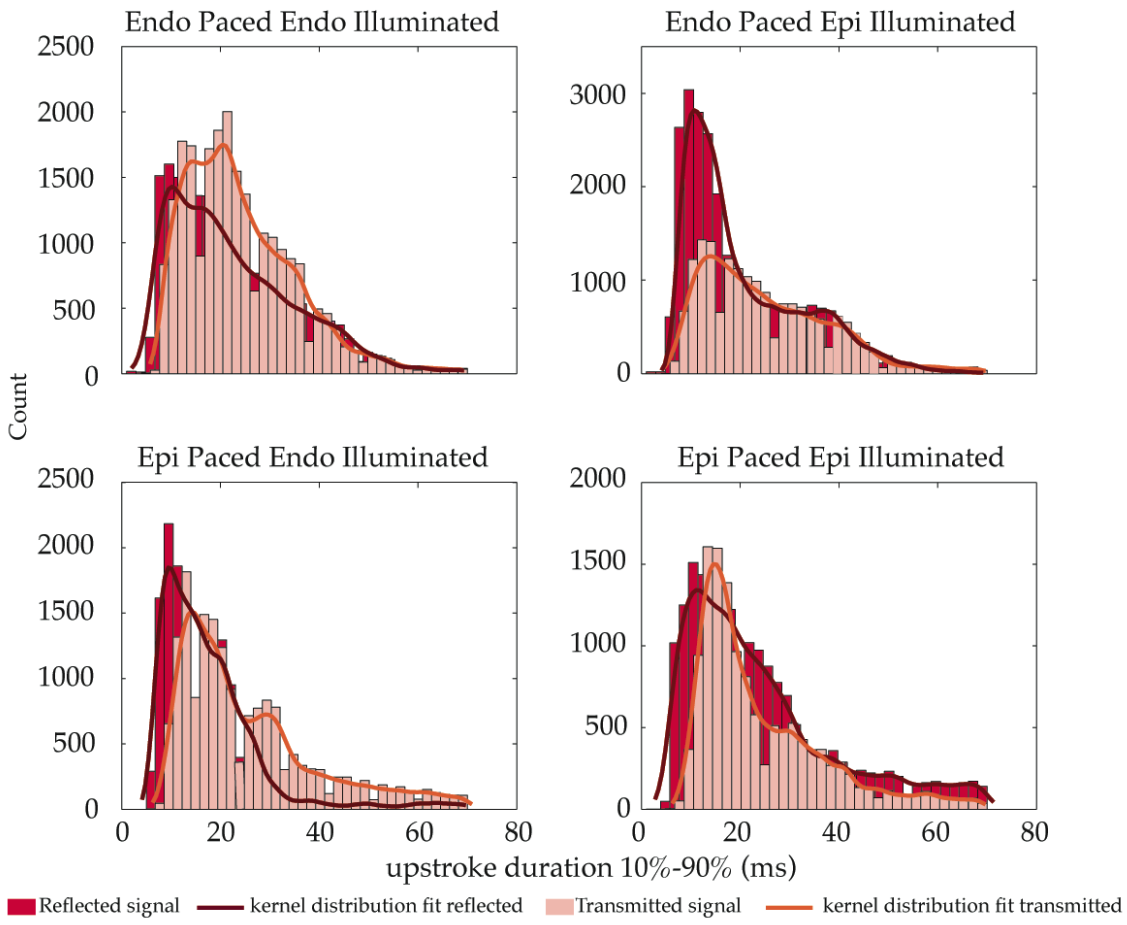

Supplemental Figure 2:

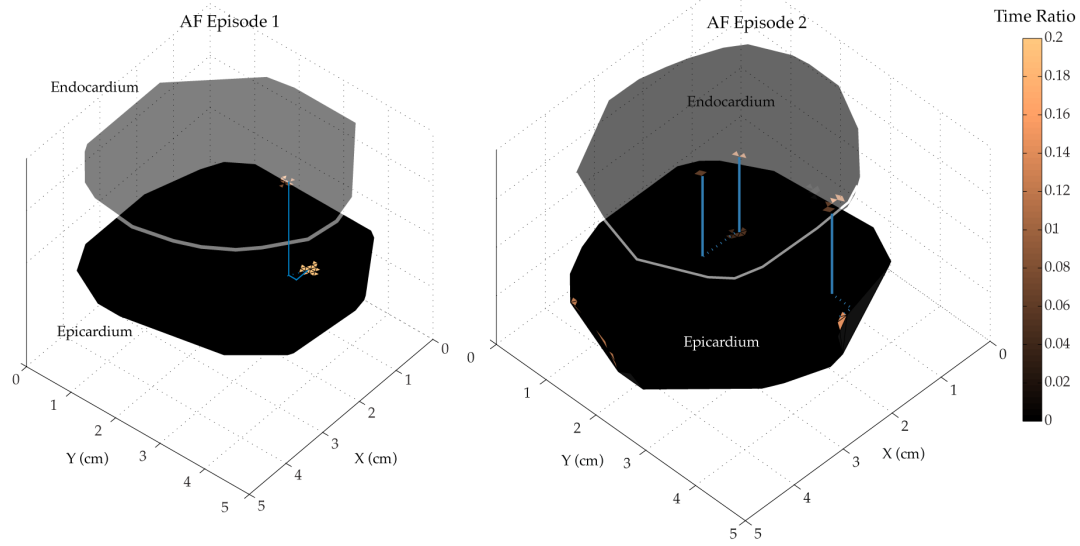

Supplemental Figure 3:

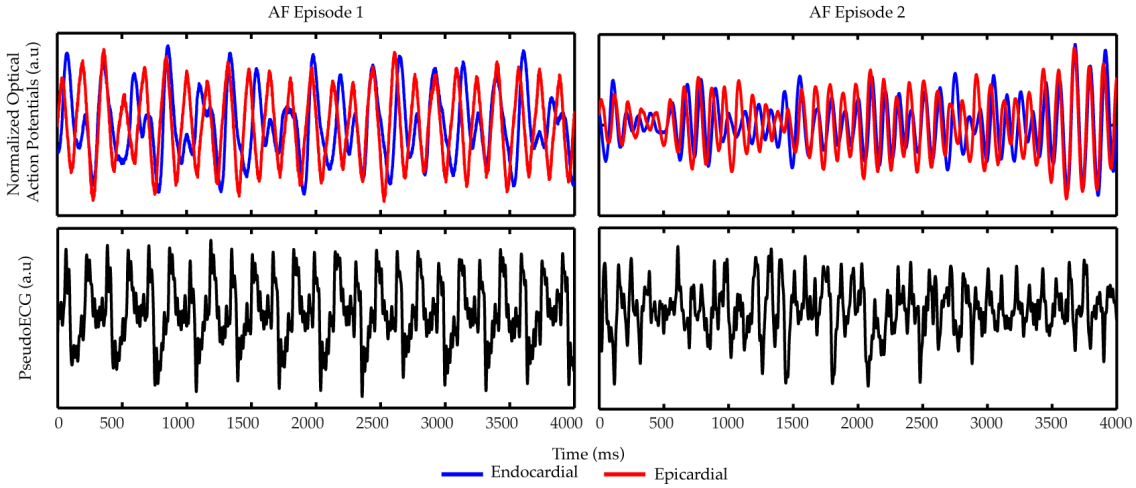

Supplemental Figure 4:

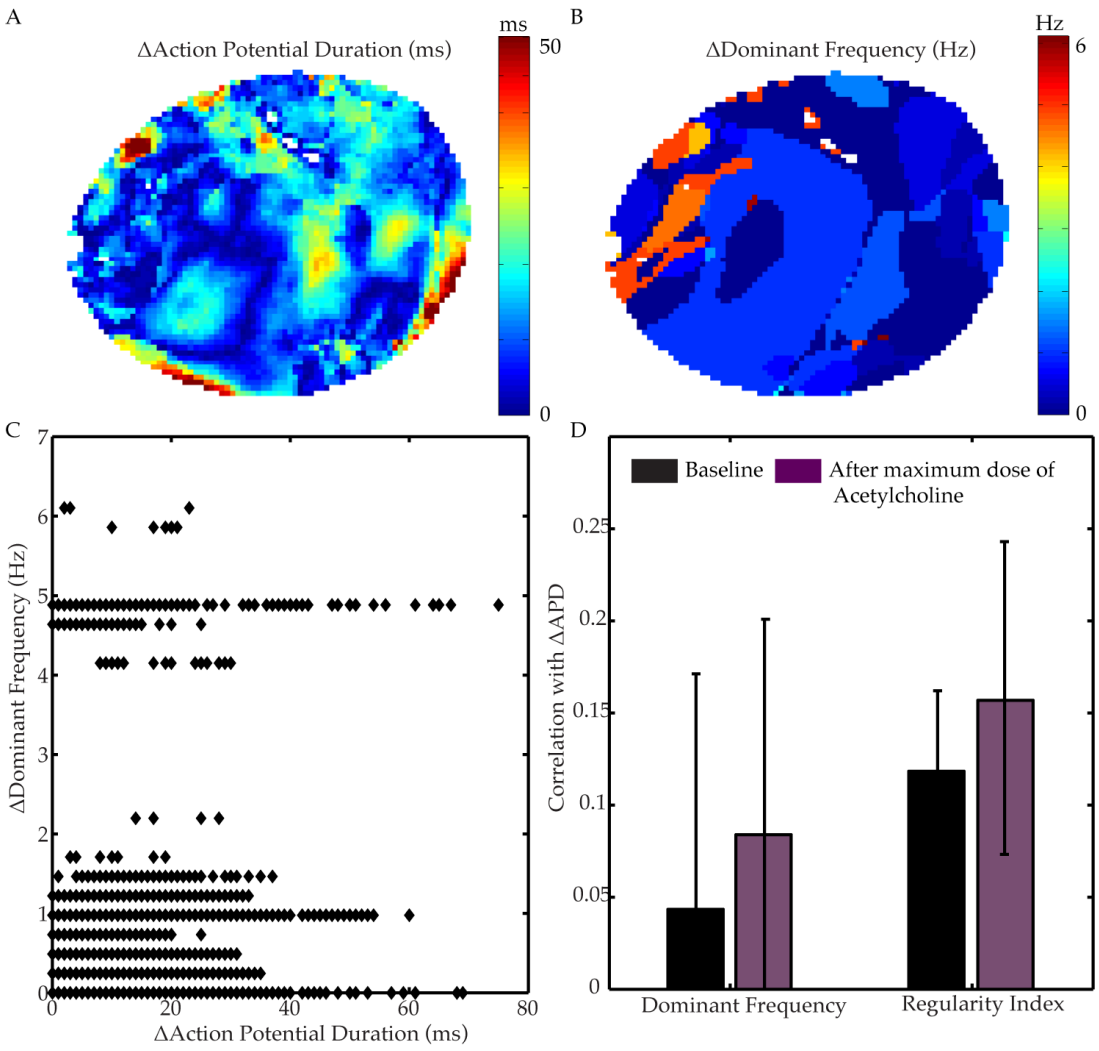

Figure Legends:

Supplemental Figure 1: Distribution of Upstroke Duration: Histograms of upstroke durations during 2Hz pacing from two imaging planes in a variety of configurations. The right shift of the distribution for transilluminated signals supports the claim that the second plane is a deeper signal.

Supplemental Figure 2: Phase Singularity Incidence Map: Representative phase singularity incidence map for a single rotor AF episode. A threshold is applied to include phase singularities that are present at least 10% of the total sequence. The blue lines represent the distance between nearest neighbor PS on the opposing imaging plane.

Supplemental Figure 3: Representative Signals from Atrial Fibrillation Episodes: Normalized optical signals from corresponding pixels on the endocardial (blue) and epicardial (red) imaging plane and ECG bath (black) for the two detailed AF episodes. The simultaneous potential traces highlight moments of dyssynchrony across the transmural wall.

Supplemental Figure 4: APD Wall Gradient and Frequency Content Correlation: A) Representative spatial map of the differences in action potential duration across the wall after the acetylcholine was administered. **B)** Representative spatial map of dominant frequency differences across the wall during atrial fibrillation. **C)** Example correlation between A and B. **D)** Summary APD correlations with dominant frequency and regularity index wall differences from N=3 hearts showing there is no correlation.

Video Titles

Video 1: Phase map with wavefront (white line) of AF episode 1 (a discordant example).

Video 2: Potential map of AF Episode 1 (a discordant example).

Video 3: Phase map with wavefront (white line) of AF episode 2 (a transmurally well conserved example).

Video 4: Potential map of AF episode 2 (a transmurally well conserved example).